cells

MDPI

Article

Rapid Generation of Ventral Spinal Cord-like Astrocytes from Human iPSCs for Modeling Non-Cell Autonomous Mechanisms of Lower Motor Neuron Disease

Vincent Soubannier [1,2], Mathilde Chaineau [2], Lale Gursu [2], Ghazal Haghi [2], Anna Kristyna Franco Flores [2], Guy Rouleau [1], Thomas M. Durcan [1,2] and Stefano Stifani [1,*]

[1] Department of Neurology and Neurosurgery, Montreal Neurological Institute-Hospital, McGill University, Montreal, QC H3A 2B4, Canada; vincent.soubannier@mcgill.ca (V.S.); guy.rouleau@mcgill.ca (G.R.); thomas.durcan@mcgill.ca (T.M.D.)

[2] Early Drug Discovery Unit, Montreal Neurological Institute-Hospital, McGill University, Montreal, QC H3A 2B4, Canada; mathilde.chaineau@mcgill.ca (M.C.); lale.gursu@mail.mcgill.ca (L.G.); ghazal.haghi@mcgill.ca (G.H.); anna.francoflores@mcgill.ca (A.K.F.F.)

* Correspondence: stefano.stifani@mcgill.ca

Abstract: Astrocytes play important roles in the function and survival of neuronal cells. Dysfunctions of astrocytes are associated with numerous disorders and diseases of the nervous system, including motor neuron diseases such as amyotrophic lateral sclerosis (ALS). Human-induced pluripotent stem cell (iPSC)-based approaches are becoming increasingly important for the study of the mechanisms underlying the involvement of astrocytes in non-cell autonomous processes of motor neuron degeneration in ALS. These studies must account for the molecular and functional diversity among astrocytes in different regions of the brain and spinal cord. It is essential that the most pathologically relevant astrocyte preparations are used when investigating non-cell autonomous mechanisms of either upper or lower motor neuron degeneration in ALS. Here, we describe the efficient and streamlined generation of human iPSC-derived astrocytes with molecular and biological properties similar to physiological astrocytes in the ventral spinal cord. These induced astrocytes exhibit spontaneous and ATP-induced calcium transients, and lack signs of overt activation. Human iPSC-derived astrocytes with ventral spinal cord features offer advantages over more generic astrocyte preparations for the study of both ventral spinal cord astrocyte biology and the involvement of astrocytes in mechanisms of lower motor neuron degeneration in ALS.

Keywords: amyotrophic lateral sclerosis; astrocyte; human-induced pluripotent stem cells; lower motor neuron; spinal cord

Citation: Soubannier, V.; Chaineau, M.; Gursu, L.; Haghi, G.; Franco Flores, A.K.; Rouleau, G.; Durcan, T.M.; Stifani, S. Rapid Generation of Ventral Spinal Cord-like Astrocytes from Human iPSCs for Modeling Non-Cell Autonomous Mechanisms of Lower Motor Neuron Disease. *Cells* **2022**, *11*, 399. https://doi.org/10.3390/cells11030399

Academic Editor: Jason Ear

Received: 20 December 2021
Accepted: 21 January 2022
Published: 24 January 2022

1. Introduction

Astrocytes are a morphologically and functionally heterogeneous group of glial cells in the mammalian nervous system. They perform a number of functions, such as structural and trophic support of neurons, homeostasis of the blood–brain barrier, participation in synaptogenesis and plasticity, and involvement in neuroinflammatory processes [1–3]. Astrocytes in different regions of the nervous system exhibit morphological and functional diversity, reflecting their specific developmental origins and integration into different cellular microenvironments in the brain or spinal cord [4–9]. The most frequently described example of morphological diversity among astrocytes is the presence of two major subtypes, termed protoplasmic and fibrous astrocytes, which are typically located in the gray matter and white matter, respectively [4–9]. These morphological differences are associated with molecular and functional diversity. Specifically, protoplasmic astrocytes are in close contact with synapses and actively regulate synapse formation, maturation and function. On the other hand, white matter fibrous astrocytes are involved in mechanisms underlying axonal

biology and myelination [9–12]. These functional diversities are correlated with defined molecular traits. For instance, protoplasmic and fibrous astrocytes differ in the expression level of the intermediate filament protein, glial fibrillary acidic protein (GFAP), which is significantly higher in fibrous astrocytes than in protoplasmic astrocytes [8–12].

The existence of multiple types of astrocytes with diverse molecular properties and functions underscores the importance of selecting the most informative experimental model systems when investigating defined biological mechanisms involving astrocytes in the developing and adult nervous system. Achieving this objective is particularly challenging when studying the roles of human astrocytes in health and disease, given the recognized difficulties in establishing primary cultures of human astrocytes. The advent of induced pluripotent stem cell (iPSC)-based approaches has addressed some of these limitations by providing efficient and reliable approaches to generate physiologically relevant human astrocytes (e.g., [13–17], to cite only a few previous studies). However, the diversity of astrocytes along the different axes of the nervous system poses a significant challenge to research aiming to investigate the multiple roles of astrocytes using cells derived from human iPSCs. The success of these investigations depends in large part on the ability to generate the specific astrocyte subtypes that are physiologically relevant to the biological processes under study, in both healthy and diseased conditions.

A compelling example of the importance of studying the appropriate astrocyte subtypes in the right context is provided by amyotrophic lateral sclerosis (ALS), a motor neuron disease that causes the degeneration of both brain (upper) and brainstem/spinal cord (lower) motor neurons [18–21]. Motor neuron degeneration in ALS is not only caused by cell-autonomous cell death mechanisms but can also result from non-cell autonomous processes involving non-neuronal cells, including astrocytes [22–24]. It is believed that astrogliosis induced in response to initial insults to motor neurons plays neuroprotective roles at first, but then gradually progresses towards neuroinflammatory functions that exacerbate neuronal degeneration. It is hypothesized that astrocytes exert deleterious effects on motor neurons in ALS as a consequence of either the loss of supportive functions or gain of toxic functions (or a combination of both) [22–27]. Upper and lower motor neurons interact with specific subgroups of astrocytes found in either the dorsal forebrain or ventral brainstem/spinal cord, respectively. The specialized cross-talk of defined motor neurons with particular astrocyte subtypes contributes to the different functions performed by upper and lower motor neurons, and is believed to also play roles in the mechanisms of upper or lower motor neuron degeneration [28–30]. Thus, understanding the contributions of human astrocytes to upper and lower motor neuron degeneration necessitates the implementation of experimental strategies that can generate pathophysiologically relevant astrocyte subtypes with the appropriate rostrocaudal and dorsoventral identities [31]. In this regard, available protocols to derive astrocytes with validated characteristics of astrocytes located in the ventral half of the spinal cord (ventral spinal cord astrocytes) are scarce and time consuming [31].

Here, we describe a protocol enabling the efficient and timesaving generation from human iPSCs of astrocytes displaying molecular and biological properties of ventral spinal cord astrocytes. These cells are expected to provide an advanced experimental model system for the study of spinal cord astrocyte biology and the involvement of astrocytes in the mechanisms of lower motor neuron degeneration in ALS and other motor neuron diseases.

2. Materials and Methods

2.1. Human-Induced Pluripotent Stem Cells

Human iPSC line AIW002-02 was established from peripheral blood mononuclear cells obtained from a 37-year-old male through retrovirus reprogramming using the CytoTune-iPS 2.0 Sendai Reprogramming kit (Thermo-Fisher Scientific; Waltham, MA, USA; Cat. No. A16518) [32]. The cell line was established at the Montreal Neurological Institute-Hospital through procedures conducted under Ethical Review Board approval by the McGill University Health Centre. Similar studies were conducted using more than one

human iPSC line, resulting in similar results. Undifferentiated state of human iPSCs was routinely assessed by testing for expression of the stem cell markers NANOG and OCT4 and by quality control profiling, as described previously [32].

2.2. Derivation of Neural Progenitor Cells from Human iPSCs

Human iPSCs at low passage number were cultured in mTeSR medium (STEMCELL Technologies; Vancouver, BC, Canada; Cat. No. 85850) in 10 cm culture dishes (Thermo-Fisher Scientific; Cat. No. 353003) coated with Matrigel (Thermo-Fisher Scientific; Cat. No. 08-774-552) until they reached 70–80% confluence. To generate neural progenitor cells (NPCs), iPSCs were dissociated with Gentle Cell Dissociation Reagent (STEMCELL Technologies; Cat. No. 07174), followed by seeding of $2 - 3 \times 10^6$ cells onto T25 flasks (Thermo-Fisher Scientific; Cat. No. 12-556-009), coated with Matrigel, in the presence of 5 mL of 'neural induction medium' containing DMEM/F12 supplemented with GlutaMax (1/1; Thermo-Fisher Scientific; Cat. No. 10565-018), neurobasal medium (1/1; Thermo-Fisher Scientific; Cat. No. 21103-049), N2 (0.5X; Thermo-Fisher Scientific; Cat. No. 17504-044), B27 (0.5X; Thermo-Fisher Scientific; Cat. No. 17502-048), ascorbic acid (100 µM; Sigma-Aldrich; St. Louis, MO, USA; Cat. No. A5960), L-Glutamax (0.5X; Thermo-Fisher Scientific; Cat. No. 35050-061), antibiotic–antimycotic (1X; Thermo-Fisher Scientific; Cat. No. 15240-062), 3 µM CHIR99021 (Selleck Chemicals; Houston, TX, USA; Cat. No. S2924), 2 µM DMH1 (Selleck Chemicals; Cat. No. S7146), 2 µM SB431542 (Selleck Chemicals; Cat. No. S1067), and 10 µM ROCK inhibitor (compound Y-27632 2HCl; Selleck Chemicals; Cat. No. S1049). After 24 h, the medium was replaced with the same medium without ROCK inhibitor. The culture medium was changed every other day until day in vitro 6 (DIV6), when induced NPCs were instructed to acquire a caudalized and ventralized progenitor cell identity as described [33,34]. Briefly, NPCs were dissociated with Gentle Cell Dissociation Reagent and split 1:6 in NPC expansion medium composed of the same medium described above, supplemented with retinoic acid (RA) (0.1 µM; Sigma-Aldrich; Cat. No. R2625) and purmorphamine (0.5 µM; Sigma-Aldrich; Cat. No. SML-0868) in combination with 1 µM CHIR99021, 2 µM DMH1 and 2 µM SB431542 reagents. The culture medium was changed every other day until DIV12, when they were split again 1:6 and expanded with the same medium containing 3 µM CHIR99021, 2 µM DMH1, 2 µM SB431542, 0.1 µM RA, 0.5 µM purmorphamine, and 500 µM valproic acid (VPA; Sigma-Aldrich; Cat. No. P4543) till DIV19. The ensuing caudalized and ventralized NPCs were validated by real-time polymerase chain reaction (RT-PCR) and immunocytochemistry.

2.3. Differentiation of Astrocytes from Human iPSC-Derived Neural Progenitor Cells

Induced caudalized and ventralized NPCs were differentiated into astrocytes starting at DIV19 using a defined medium, essentially as described previously [17]. NPCs were seeded at low cell density (15,000 cells/cm^2) in two T25 flasks in the presence of 5 mL of NPC expansion medium containing ROCK inhibitor. The next day, medium was replaced with 'Astrocyte Differentiation Medium 1' (ScienCell Astrocyte Growth Medium (ScienCell Research Laboratories; Carlsbad, CA, USA; Cat. No. 1801b) containing astrocyte growth supplement (ScienCell Research Laboratories; Cat. No. 1852), 1% fetal bovine serum (FBS) (ScienCell Research Laboratories; Cat. No. 0010), 50 U/mL penicillin G, 50 mg/mL streptomycin). Cells were split 1:4 every week and were maintained under these culture conditions for 30 days. Half medium was replaced with fresh medium every 3 to 4 days. At DIV50, cultures were switched to 'Astrocyte Differentiation Medium 2' (same as Astrocyte Differentiation Medium 1 but lacking FBS), and routinely analyzed at DIV80. Induced astrocytes were validated by immunocytochemistry, RT-PCR, and calcium imaging.

2.4. Characterization of Induced Cells by Immunocytochemistry

Induced human NPCs and astrocytes were analyzed by immunocytochemistry, which was performed as described previously [35]. The following primary antibodies were used: anti HOXA5 and anti-HOXC9 (1/67,000, kindly provided by Dr. Jeremy Dasen,

New York, NY, USA, University School of Medicine), rabbit anti-FOXG1 (1/300; Abcam; Cat. No. Ab196868), mouse anti-NKX6.1 (1/500; DSHB; Cat. No. F55A10), rabbit anti-PAX6 (1/500; BioLegend; Cat. No. 901301) mouse anti-GFAP (1/1000; Sigma-Aldrich; Cat. No. G3893); mouse anti-S100B (1/500; Sigma-Aldrich; Cat. No. S2532); mouse anti-GAP JUNCTION PROTEIN ALPHA 1 (GJA1) (1/500; Abcam; Cat. No. 11369), and rabbit anti-SLC1A2/EAAT2/GLT-1 (SLC1A2) (1/500; Abcam; Cat. No. 41621). The indicated DSHB monoclonal antibodies were obtained from the Developmental Studies Hybridoma Bank, created by the NICHD of the NIH and maintained at the University of Iowa, Department of Biology, Iowa City, IA 52242, USA. Secondary antibodies against primary reagents raised in various species were conjugated to Alexa Fluor 555 and Alexa Fluor 488 (1/1000; Invitrogen; Burlington, ON, Canada). Actin polymerization was visualized by staining of F-actin using Alexa-Fluor-488 phalloidin (1/500; Thermo Fisher; Cat. No. A12379). Images were acquired with a Zeiss Axio Observer Z1 Inverted Microscope using 20× magnification (N.A 0.8) and a ZEISS Axiocam 506 mono camera. Quantification of the proportion of cells expressing a specific marker was performed by counting the number of cells presenting a positive labeling of the marker and dividing it by the total number of Hoechst-positive nuclei.

2.5. Characterization of Induced Cells by Real-Time Polymerase Chain Reaction

RNA extraction and real-time polymerase chain reaction (RT-PCR) were performed as described [36]. Analysis of gene expression was conducted using the following oligonucleotide primers: Taqman probes *FOXG1*, Hs01850784_s1; *HOXA3*, Hs00601076_m1; *HOXA5*, Hs00430330_m1; *HOXB8*, Hs00256885_m1; *NKX2.2*, Hs00159616_m1; *NKX6.1*, Hs00232355_m1; *NKX6.2*, Hs00752986_s1; *PAX6*, Hs01088114_m1; *PAX3*, Hs00240950_m1; *PAX7*, Hs00242962_m1; *GFAP, Hs00909233_m1*; *S100B*, Hs00902901_m1; *CD44*, Hs01075864_m1; *GJA1*, Hs00748445_s1; *SLC1A2*, Hs01102423_m1; *SLC1A3/EAAT1/GLAST (EAAT1), Hs00904823_g1; AQUAPORIN-4 (AQP4), Hs00242342_m1; TFAP2A*, Hs01029413_m1; *REELIN*, Hs01022646_m1; *POTASSIUM INWARDLY RECTIFYING CHANNEL SUBFAMILY J MEMBER 10* (*KCNJ10*), Hs00158426_m1; *AMIGO2*, Hs00827141_g1; *SERGLYCIN*, *Hs01004159_m1; COMPLEMENT C1S (C1S*), Hs00156159_m1; *COMPLEMENT C3* (*C3*), Hs00163811_m1; *INTERLEUKIN-1BETA* (*IL-1β), Hs01555410_m1; TUMOR NECROSIS FACTOR ALPHA (TNF-α), Hs 00174128_m1; C-C MOTIF CHEMOKINE LIGAND 2 (CCL2*), Hs00234140_m1; *C-X-C MOTIF CHEMOKINE LIGAND 10* (*CXCL10*), Hs00171042_m1). Primer/probe sets were obtained from ThermoFisher Scientific. Data were normalized with *BETA-ACTIN* and *GAPDH* (*ACTB Hs01060665_g1; GAPDH Hs02786624_g1).* Relative quantification (RQ) was estimated according to the ΔCt method; the ratio between the RQ of cells with spinal cord (SC) identity over the RQ of cells with forebrain identity was calculated using the ΔΔCt method ([37] and references therein).

2.6. Detection of Calcium Transients in Human iPSC-Derived Astrocytes

DIV80 human iPSC-derived astrocytes were incubated with the calcium indicator Fluo-4 AM (1 μM; ThermoFisher Scientific; Cat. No. F14201) for 30 min, followed by two rinsing steps with ScienCell Astrocyte Growth Medium, supplemented with antibiotics, for 10 min each. Time-lapse microscopy was then performed at 0.5 Hz with a Zeiss Axio Observer Z1 Inverted Microscope using 20× magnification (numerical aperture 0.8) and a ZEISS Axiocam 506 mono camera. Temperature (37 °C), humidity, and CO_2 (5%) were maintained at constant levels throughout the course of the experiments through TempModule S and CO_2 Module S devices (PeCon GmbH; Erbach, Germany). LED 488 nm was set at 20% and exposure time was 200 ms to avoid phototoxicity. For spontaneous calcium wave acquisition, recording was conducted for 5 min and focus stabilisation was achieved with the use of Zeiss Definite focus every 30 images. For induced calcium wave acquisition, recording was performed for 1 min, before the addition of 10 μM ATP, followed by an additional 4 min recording. Analysis of at least 25 cells per acquisition video was performed using the calcium signaling analyzer tool, CaSiAn [38].

3. Results

3.1. Generation of Caudalized and Ventralized Neural Progenitor Cells from Human iPSCs

To generate human iPSC-derived NPCs with the potential to give rise to cells with properties of ventral spinal cord astrocytes, iPSCs were first instructed to undergo neural induction in vitro by inhibiting BMP/TGFβ signaling pathways for 6 days using a combination of the small molecules CHIR99021, DMH1 and SB431542. The ensuing NPCs were exposed to ventralizing and caudalizing cues by combined treatment with 0.5 μM purmorphamine and 0.1 μM RA for 6 additional days, as previously described [33,34], followed by NPC expansion till DIV19 (Figure 1A).

Immunocytochemistry and RT-PCR studies were performed to confirm the generation of NPCs with caudal (e.g., brainstem/spinal) and ventral neural tube properties. RT-PCR showed that three transcripts associated with caudal positional identity, such as *HOXA3*, *HOXA5*, and *HOXB8* [39–41], were expressed in NPCs exposed to purmorphamine and RA ('purmorphamine/RA' hereafter) (Figure 1B). To complement this observation, we examined the expression of *FOXG1*, a marker of forebrain NPCs [42]. *FOXG1* transcript level was below the limit of detection (Figure 1B). The expression levels of these genes in caudal (e.g., brain stem/spinal cord) NPCs generated in the presence of purmorphamine and RA were compared with the levels in forebrain NPCs generated without these reagents, as previously described [36]. Expression of the rostral marker *FOXG1* was considerably higher in NPCs with forebrain identity (Figure 1C). In contrast, all three caudal markers, *HOXA3*, *HOXA5*, and *HOXB8*, were highly expressed in brain stem/spinal cord ('spinal cord' hereafter) NPCs compared with forebrain NPCs (Figure 1D). In agreement with these findings, immunocytochemistry showed that the majority of spinal cord NPCs expressed the proteins HOXA5 (96.1% ± 1.5%) and HOXC9 (another caudal *HOX* gene product) (99.3% ± 1.2%), but were negative for nuclear FOXG1 expression (Figure 1E).

To validate the ventral identity of NPCs exposed to purmorphamine/RA, we examined the expression of genes marking ventral and dorsal NPCs in the spinal cord in vivo, including *NKX2.2*, *NKX6.1*, *NKX6.2*, *PAX6*, *PAX3* and *PAX7* [43–45]. This analysis showed detectable expression of the exclusively, or predominantly, ventral markers *NKX2.2*, *NKX6.1*, and *NKX6.2*, as well as *PAX6*, which marks both ventral and dorsal spinal cord progenitor domains in vivo; in contrast, the predominantly dorsal markers *PAX3* and *PAX7* were undetectable (Figure 1F). Comparison of the expression levels of the ventral markers *NKX2.2* and *NKX6.1* in spinal cord and forebrain NPCs showed that the latter were more robustly expressed in NPCs with spinal cord identity (Figure 1G). Immunocytochemistry confirmed that most of the spinal cord NPCs expressed NKX6.1 (91% ± 1.5%) and PAX6 (93.3% ± 1.9%) (Figure 1H). Together, these results demonstrate the robust generation of NPCs with caudal and ventral characteristics from human iPSCs by DIV19.

3.2. Generation of Astrocytes from Caudalized and Ventralized Neural Progenitor Cells

NPCs characterized as described above were induced to undergo astrocytic commitment and differentiation in vitro starting at DIV20. The expression of common astrocyte marker genes, such as *GFAP*, *S100B*, and *VIMENTIN*, was detected in differentiating cultures as early as DIV50 (not shown). At DIV80, most induced cells displayed a fibrous morphology characterized by long and thin extensions (Figure 2A) and were positive for S100B (95.2% ± 0.6%) and GFAP (70.9% ± 5.8%) expression (Figure 2B). A fraction (30.7% ± 2.2%) of GFAP-positive cells displayed a high level of expression, with the remaining cells exhibiting lower GFAP immunoreactivity (Figure 2B). Induced cells expressed other typical astrocyte marker genes, such as *GJA1* (also referred to as *CONNEXIN-43*), *SLC1A2* (also known as *EXCITATORY AMINO ACID TRANSPORTER 2—EAAT2*) (albeit at low level), *SLC1A3* (also known as, *EAAT1*), and *CD44* (Figure 2C–E), confirming their astrocytic molecular identity.

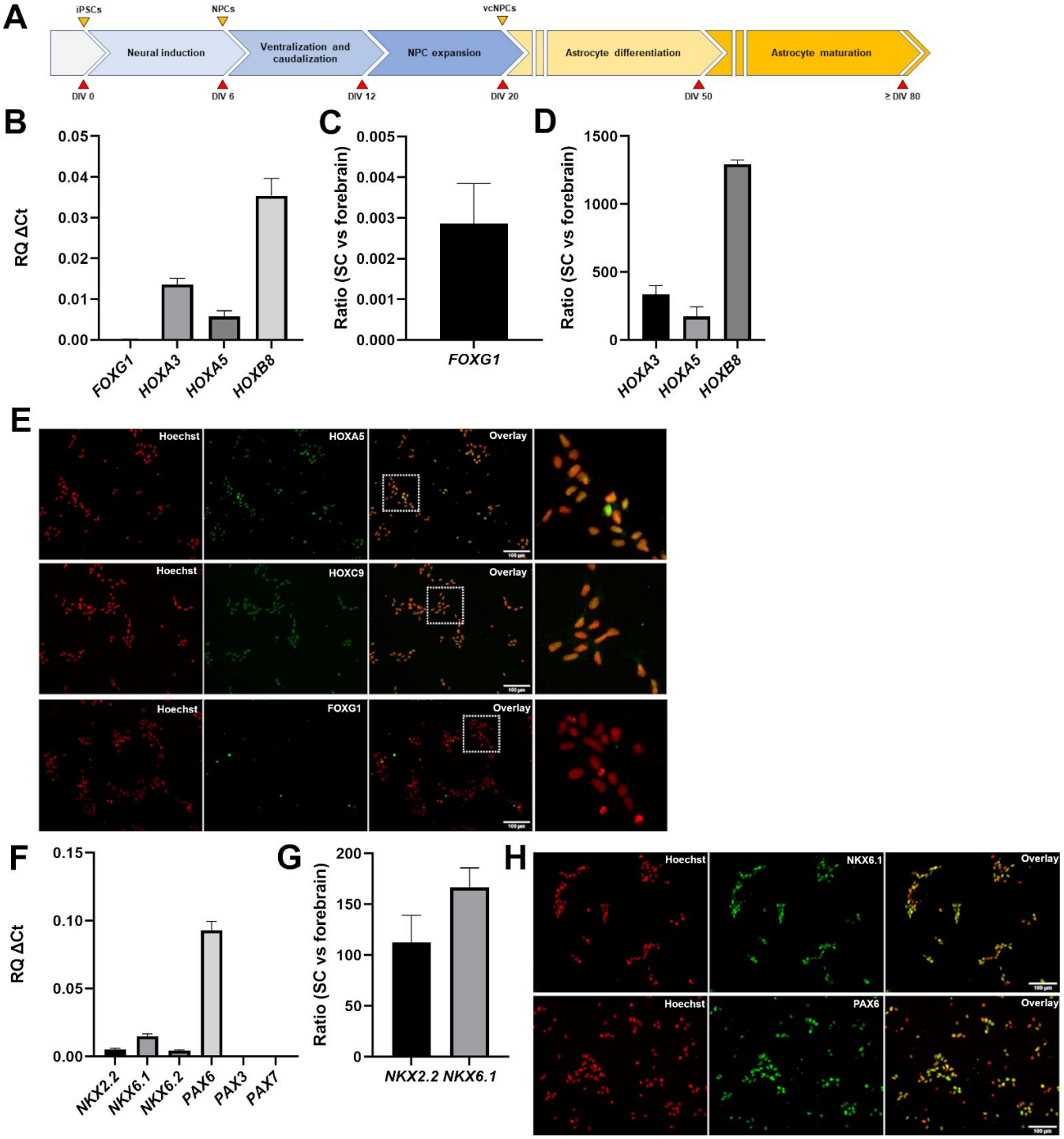

Figure 1. Generation and characterization of ventralized and caudalized neural progenitor cells. (**A**) Schematic representation of the main steps of the differentiation protocol used to generate caudalized and ventralized neural progenitor cells and astrocytes. Days in vitro (DIV) are indicated. NPCs, neural progenitor cells; vcNPCs, ventralized and caudalized neural progenitor cells. (**B**) Real-time PCR analysis of the expression of forebrain marker *FOXG1* and caudal markers *HOXA3*, *HOXA5*, and *HOXB8* in NPCs at DIV19. (**C**) $2^{-\Delta\Delta CT}$ analysis depicting the ratio of *FOXG1* expression in ventral spinal cord ('SC') NPCs and forebrain NPCs. (**D**) $2^{-\Delta\Delta CT}$ analysis depicting the ratio of the expression of the indicated genes in ventral spinal cord ('SC') NPCs and forebrain NPCs. (**E**) Representative images of immunofluorescence analysis of induced NPCs, showing that most of the cells are positive for HOXA5 and HOXC9 (green), but negative for FOXG1, at DIV19; Hoechst counterstaining (red) is

shown. In each row, dotted-line box in the third panel indicates area shown at higher magnification in the fourth panel on the right-hand side. (**F**) Real-time PCR analysis of the expression of a panel of ventral-to-dorsal spinal cord markers, namely *NKX2.2*, *NKX6.1*, *NKX6.2*, *PAX6*, *PAX3* and *PAX7* in ventral spinal cord NPCs. (**G**) $2^{-\Delta\Delta CT}$ analysis depicting the ratio of the expression of the indicated genes in ventral spinal cord ('SC') NPCs and forebrain NPCs. (**H**) Representative images of immunofluorescence analysis of induced NPCs, showing that most cells are positive for NKX6.1 and PAX6 (green) at DIV19; Hoechst counterstaining (red) is shown.

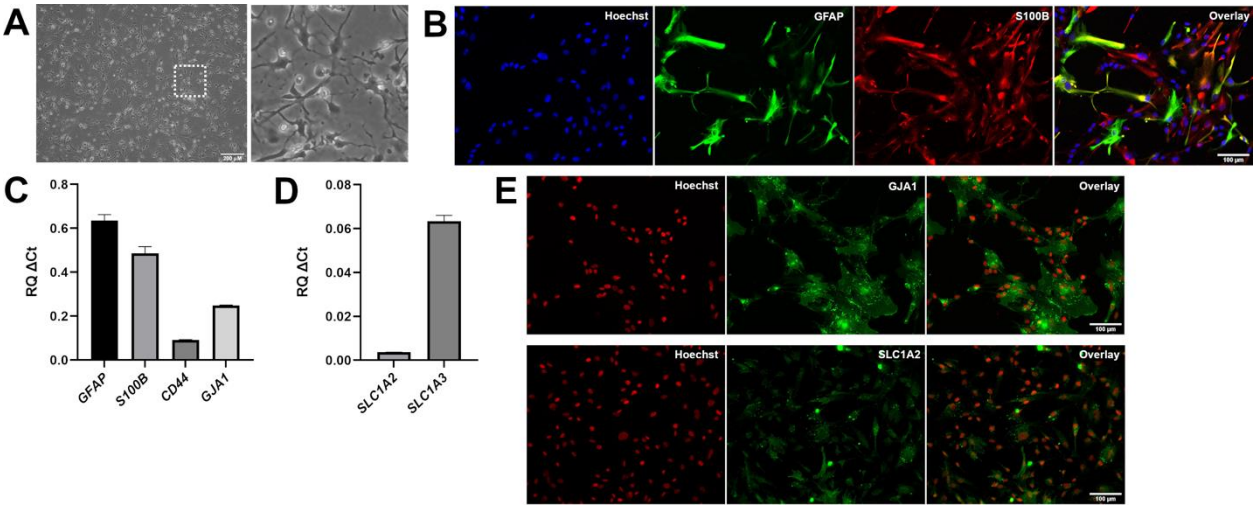

Figure 2. Characterization of astrocytes generated from ventralized and caudalized neural progenitor cells. (**A**) Phase contrast image of DIV80 astrocytes derived from ventralized and caudalized NPCs, showing that most cells have stellate-like morphologies with long and thin extensions. Box in left-hand panel indicates area shown at higher magnification in right-hand panel. (**B**) Representative double-labeling immunofluorescence analysis of GFAP (green) and S100B (red) expression in DIV80 astrocytes; Hoechst counterstaining (blue) is shown. The majority of induced cells express S100B, and a significant proportion of S100B-positive cells co-express GFAP at high level, while other S100B-positive cells co-express GFAP at low level. (**C**,**D**) Real-time PCR analysis of the expression of *GFAP*, *S100B*, *CD44*, *GJA1* (**C**), as well as *SLC1A2* and *SLC1A3* (**D**) in induced astrocytes. (**E**) Immunofluorescence analysis of GJA1 and SLC1A2 (green) expression in DIV80 astrocytes generated from ventralized and caudalized NPCs; Hoechst counterstaining (red) is shown.

The caudalized nature of the astrocytes generated from purmorphamine/RA-treated NPCs was first validated by the persistent expression of *HOXA3*, *HOXA5*, and *HOXB8*, and a lack of rostral marker *FOXG1* expression (Figure 3A). The continued expression in spinal astrocytes of *HOX* genes first expressed in their progenitors is consistent with the results of previous in vitro studies [41]. Conversely, forebrain astrocytes expressed *FOXG1* but not *HOXA3*, *HOXA5*, and *HOXB8* (Figure 3B). In agreement with these observations, astrocytes generated from purmorphamine/RA-treated NPCs also continued to express *NKX6.2* (Figure 3A), which has been previously identified as a marker of spinal cord, but not forebrain, astrocytes [41]. Quantification of the ratio of gene expression in the two types of astrocytes confirmed the forebrain astrocyte-specific expression of *FOXG1* (Figure 3C) and the enrichment of *HOXA3*, *HOXA5*, *HOXB8*, *NKX6.1* and *NKX6.2* in spinal cord astrocytes (Figure 3D).

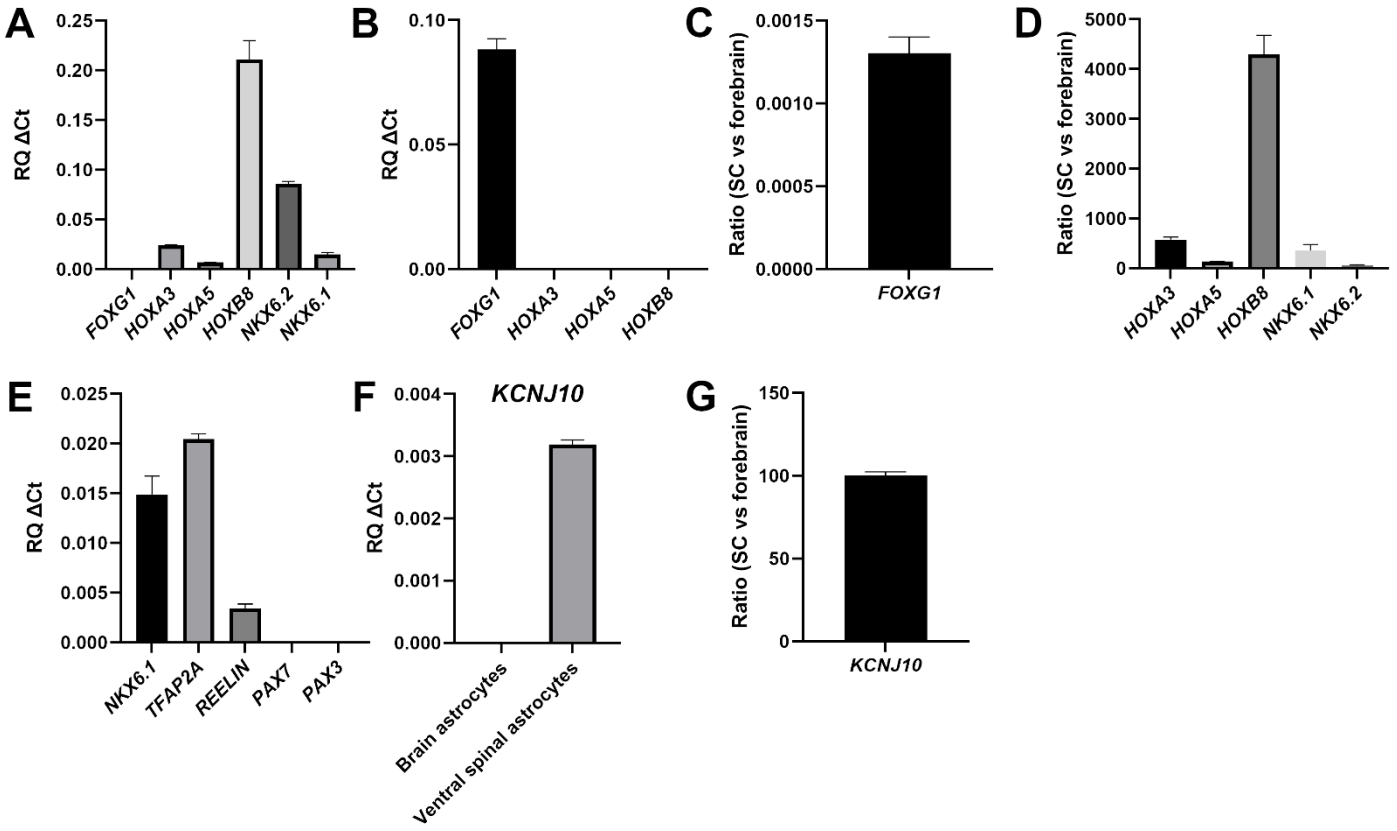

Figure 3. Characterization of human iPSC-derived VS astrocytes. (**A**,**B**) Real-time PCR analysis of the expression of the indicated markers of rostrocaudal identity in either ventral spinal cord (**A**) or forebrain (**B**) astrocytes. (**C**) $2^{-\Delta\Delta CT}$ analysis depicting the ratio of *FOXG1* expression in ventral spinal cord ('SC') astrocytes and forebrain astrocytes. (**D**) $2^{-\Delta\Delta CT}$ analysis depicting the ratio of the expression of the indicated genes in ventral spinal cord ('SC') astrocytes and forebrain astrocytes. (**E**) Real-time PCR analysis of the expression of markers of ventral spinal identity in ventral spinal cord astrocytes. (**F**) Comparison of *KCNJ10* expression in forebrain ('brain') or ventral spinal cord ('ventral spinal') astrocytes. (**G**) $2^{-\Delta\Delta CT}$ analysis depicting the ratio of *KCNJ10* expression in ventral spinal cord ('SC') astrocytes and forebrain astrocytes.

To validate the ventral phenotype of the induced astrocytes, we examined the genes *NKX6.1*, *REELIN*, and *TFAP2*, whose expression was shown to be preferentially associated with ventral, but not dorsal, spinal cord astrocytes [41,46]. All of these genes were expressed in astrocytes generated from purmorphamine/RA-treated NPCs; in contrast, no detectable expression of the dorsal markers *PAX3* and *PAX7* was observed (Figure 3E). To extend this analysis, we examined the expression of the gene encoding KCNJ10, the human counterpart of the murine inward-rectifying potassium channel Kir4.1, which is preferentially expressed in astrocytes located in the ventral horn of the rodent spinal cord in vivo [47,48]. Astrocytes generated from purmorphamine/RA-treated NPCs were positive for *KCNJ10* expression; in contrast, brain astrocytes generated in the absence of ventralizing cues [36] displayed low or undetectable *KCNJ10* expression (Figure 3F,G). Together, these results provide evidence for the robust generation from human iPSCs of astrocytes with molecular features resembling those of ventral spinal cord astrocytes. These induced cells will be referred to hereafter as human iPSC-derived 'ventral spinal cord-like' (VS) astrocytes.

3.3. Lack of Overt Signs of Activation in Human iPSC-Derived VS Astrocytes

Human iPSC-derived astrocyte preparations with the best potential to offer insight into the mechanisms of astrogliosis should not be intrinsically reactive as a result of in vitro derivation conditions. The observation that human iPSC-derived VS astrocytes express a

detectable level of *KCNJ10*, which was shown to be down-regulated in reactive astrocytes in multiple studies [49–51], suggested that VS astrocytes are not reactive. To examine this possibility further, we determined the expression levels of a variety of genes previously shown to be highly expressed in reactive astrocytes. During astrogliosis, there is a negative correlation between the expression of KCNJ10 (Kir4.1 in rodents) and AQUAPORIN-4 (AQP4), an astrocytic water channel. Both KCNJ10 and AQP4 are mainly localized to astrocytic endfeet and play important roles in potassium homeostasis and blood–brain barrier integrity [52,53]. In contrast to the down-regulation of KCNJ10 during astrogliosis [49–51], AQP4 levels increase in reactive astrocytes [52–54]. Importantly, such an inverse correlation was also observed during ALS-associated astrogliosis [55,56]. RT-PCR analysis showed that human iPSC-derived VS astrocytes expressed very low levels of *AQP4* (Figure 4A), an observation consistent with the results of previous in vitro studies showing little or no *AQP4* expression in iPSC-derived spinal astrocytes [41]. This finding suggests further that human iPSC-derived VS astrocytes are not intrinsically activated.

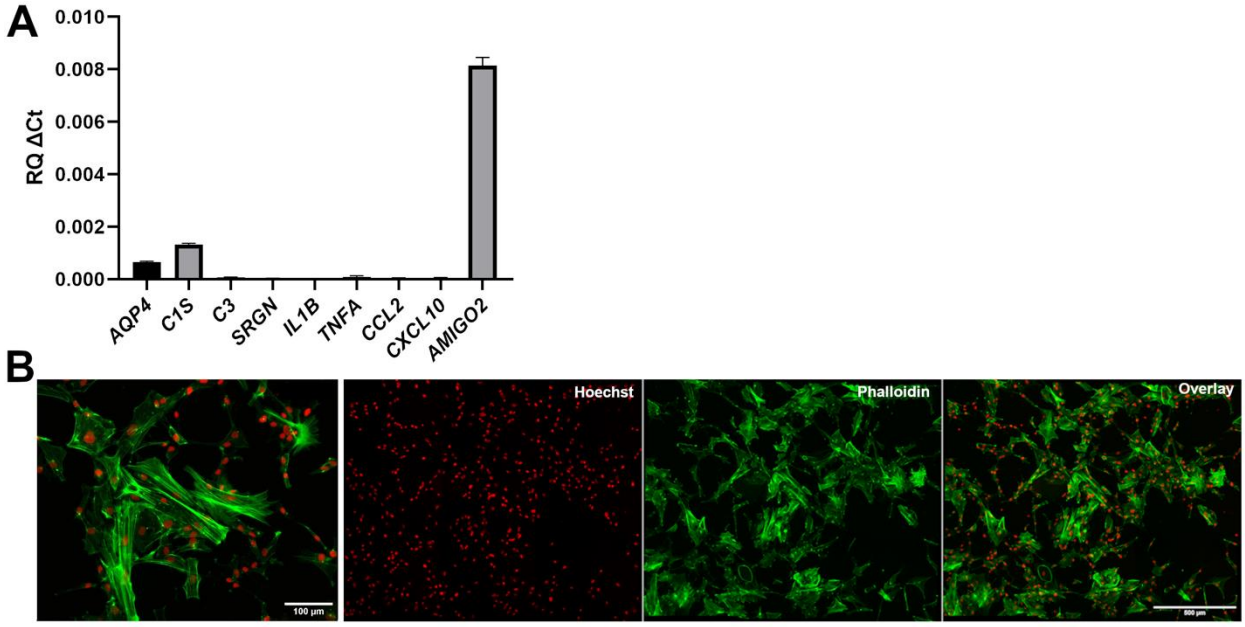

Figure 4. Lack of detectable signs of activation in human iPSC-derived ventral spinal astrocytes. (**A**) Real-time PCR analysis of the expression of a panel of astrogliosis markers. (**B**) Representative images, at different magnifications, of the actin cytoskeleton of induced astrocytes visualized by Alexa488-conjugated phalloidin staining (green); Hoechst counterstaining (red) is shown.

To extend this analysis, we next examined the expression of a number of genes associated with a reactive astrocyte phenotype in vivo and in vitro. These included complement pathway components such as *C1S* and *C3*, and the genes *SRGN*, *IL1B*, *TNFA*, *CCL2*, *CXCL10* and *AMIGO2*, all of which were reported to be up-regulated in reactive astrocytes [57–61]. RT-PCR analysis showed little or no detectable expression of most of these genes in human iPSC-derived VS astrocytes, with the exception of *AMIGO2* (Figure 4A). The latter observation is consistent with the physiological expression of *AMIGO2* in spinal cord astrocytes [62]. Of note, the levels of a number of pro-inflammatory cytokines were up-regulated when human iPSC-derived VS astrocytes were exposed to a previously described pro-reactive astrocyte phenotype medium containing TNF-α, IL-1α, and C1q [58,59], suggesting that these cells have the potential to become activated under the appropriate conditions (data not shown).

Based on these findings, we next investigated the cytoskeletal organization of human iPSC-derived VS astrocytes. It is known that F-actin stress fibers disassemble into a more disorganized G-actin network during astrogliosis, resulting in altered morphologies, also characterized by the presence of ring-like structures, ruffles, and radial actin filaments ex-

tending towards the astrocyte periphery [63,64]. DIV80 human iPSC-derived VS astrocytes displayed an organized network with discernable F-actin stress fibers using phalloidin staining (Figure 4B). Taken together, these results provide evidence suggesting that human iPSC-derived VS astrocytes are not reactive under the examined experimental conditions.

3.4. Human iPSC-Derived VS Astrocytes Display Spontaneous and ATP-Induced Calcium Waves

To further characterize the properties of human iPSC-derived VS astrocytes, and to assess their potential for the study of mechanisms of astrocyte-neuron communication, we next examined whether these preparations would exhibit spontaneous and induced cytosolic calcium [Ca^{2+}] concentration transients. Calcium concentration waves are a physiological property of functional astrocytes and represent one of the mechanisms by which astrocytes regulate neuronal functions, through the release of 'gliotransmitters' [65,66]. We incubated DIV80 human iPSC-derived VS astrocytes with the Ca^{2+} indicator Fluo-4 AM, in the absence (spontaneous Ca^{2+} transients) or presence of 10 μM ATP (induced Ca^{2+} transients) (Figure 5). Spontaneous Ca^{2+} waves were readily observed in the majority of cells, with signals frequently propagating from one cell to the adjacent ones (Figure 5A,B; Suppl. Video S1 in Supplementary Materials). Treatment with 10 μM ATP triggered a sharp increase in Ca^{2+} concentration, followed by multiple waves of calcium release, suggestive of Ca^{2+}-induced Ca^{2+} release (Figure 5D,E; Suppl. Video S2 in Supplementary Materials). We quantified Ca^{2+} transient characteristics, including amplitude, spike width, and inter-spike intervals, using CaSiAn, an open software tool [38]. The characteristics of the spontaneous and ATP-evoked Ca^{2+} waves were consistent with previous studies [17,36,38,41], further suggesting that human iPSC-derived VS astrocytes resemble physiological astrocytes (Figure 5C,F). Together, these findings provide evidence that human iPSC-derived VS astrocytes display properties such as spontaneous and evoked Ca^{2+} oscillations that are consistent with in vitro developmental maturation and suitability for the study of neuron–astrocyte communication mechanisms.

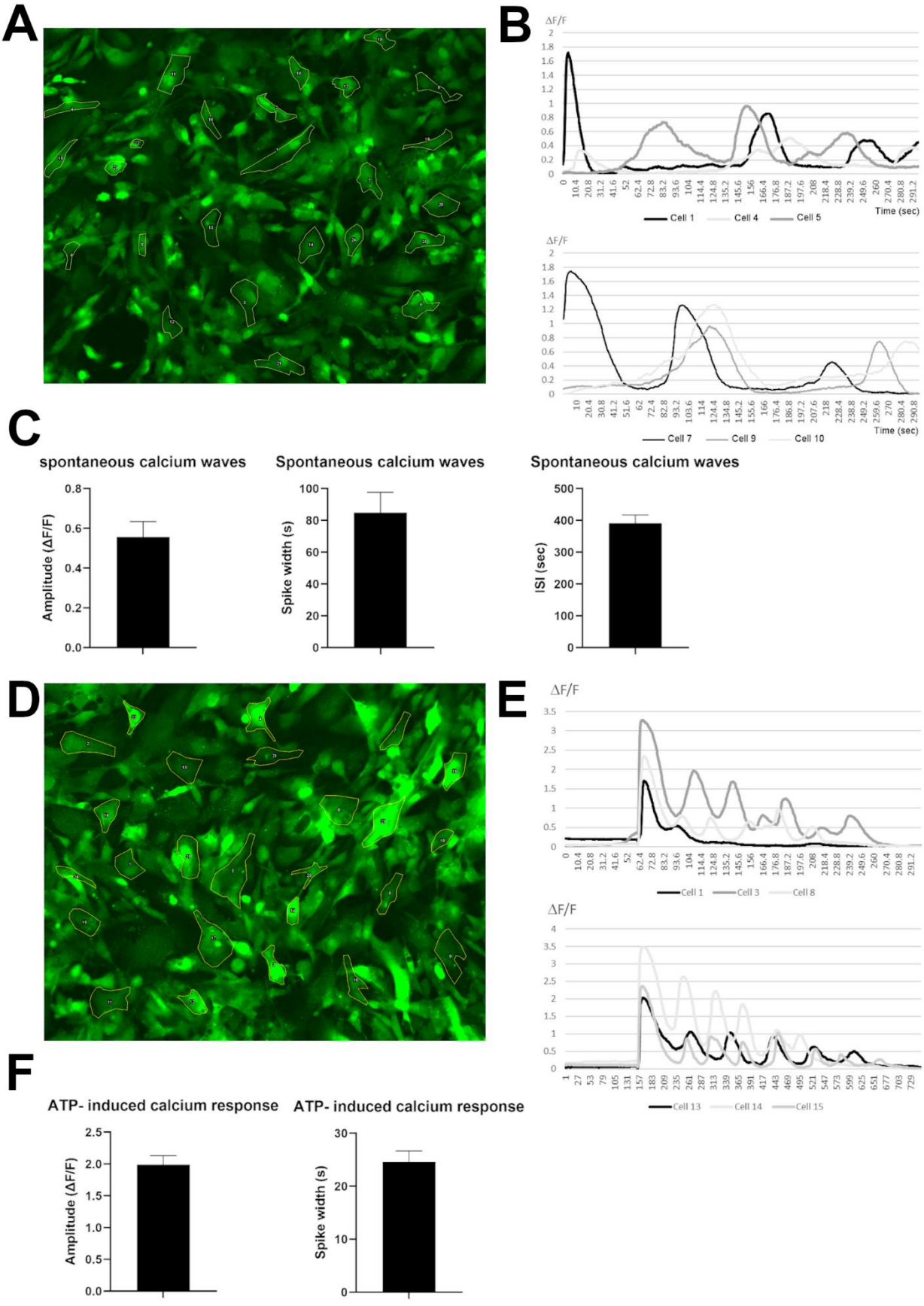

Figure 5. Spontaneous and induced calcium transients in human iPSC-derived VS astrocytes. (**A**–**C**) Analysis of spontaneous Ca^{2+} waves. (**A**) Representative Fluo-4 AM fluorescence. (**B**) ΔF/F

signals over time for 6 selected cells. (**C**) Quantification of spontaneous transients' characteristics including amplitude of signals, spike width, and interspike intervals. (**D**–**F**) Analysis of ATP-induced Ca^{2+} waves. (**D**) Representative Fluo-4 AM fluorescence. (**E**) ΔF/F signals over time for 6 selected cells. (**F**) Quantification of ATP-induced transients' characteristics including amplitude of signals, spike width, and interspike intervals.

4. Discussion

Human iPSC-derived neuronal and glial experimental model systems are becoming increasingly important to complement existing animal models to investigate the mechanisms leading to neuronal loss in neurodegenerative diseases, including ALS and other motor neuron diseases [67–70]. The success of human iPSC-based studies depends in large part on the ability to generate the specific types of neuronal and glial cells that are most relevant to the disease under study. In this regard, investigations of astrocyte involvement in ALS pathophysiology require the in vitro derivation of specific types of astrocytes with molecular and physiological properties resembling those of the astrocytes that functionally interact with motor neurons impacted by this disease. For instance, astrocytes involved in biological cross-talk with upper or lower motor neurons are not functionally equivalent to astrocytes found in areas of the nervous system where ALS-impacted neurons are not present. This situation is particularly evident in the spinal cord, where only astrocytes found in the ventral horn, where motor neurons are located, have the potential to affect motor neuron function and survival, as opposed to dorsally located spinal astrocytes [31]. Thus, astrocyte differentiation protocols aimed at investigating mechanisms of non-cell autonomous motor neuron degeneration in ALS must be optimized to generate cultures enriched for the most disease-relevant astrocyte subtypes. In this work, we have described a robust and timesaving derivation from human iPSCs of astrocytes with properties resembling those of astrocytes found in the ventral spinal cord in vivo ('human iPSC-derived VS astrocytes'). These cells exhibit a number of properties that suggest that they will offer an enhanced experimental system for the study of spinal cord astrocyte biology and non-cell autonomous mechanisms of lower motor neuron degeneration in ALS.

4.1. Human iPSC-Derived Ventral Spinal Cord-like Astrocytes Have Properties of Physiological Astrocytes

The human iPSC-based derivation protocol described in this study yields induced cells expressing a complement of typical astrocytic markers as early as 50 days after the start of the derivation process. By DIV80, many induced cells display the expression of S100B, GFAP, SLC1A2, SLC1A3, as well as GJA1, the main astrocyte gap-junction protein. More importantly, these cultures are composed of astrocytes expressing a panel of genes found in more mature astrocytes of the ventral spinal cord, including *TFAP2A*, *REELIN*, and *KCNJ10*. Conversely, they lack the detectable expression of more dorsal markers such as *PAX3* and *PAX7*. Most induced astrocytes exhibit spontaneous and induced Ca^{2+} transients by DIV80, consistent with the properties of mature astrocytes capable of functional communication with neuronal cells.

The time required to obtain robust numbers of astrocytes with the above-summarized properties is relatively rapid when compared with previous studies describing the generation and characterization of ventral spinal cord astrocytes from human iPSCs. For instance, Bradley and colleagues previously reported a ventral spinal astrocyte differentiation strategy from human iPSCs in which NPCs are first expanded in suspension for 5.5 months before differentiation to astrocytes in an adherent culture for one additional week, thus requiring almost 6 months to obtain astrocytes with the indicated properties [41]. A somewhat faster protocol, generating spinal astrocytes in about 3 months, was described by Hall and coworkers [71], but those studies, as well as others describing the generation of spinal astrocytes (e.g., [27,72,73]), did not provide a characterization of the specific ventral features of the induced astrocytes. The availability of a streamlined derivation protocol

for generating characterized ventral spinal cord-like astrocytes from human iPSCs will therefore offer an enhanced opportunity to specifically investigate mechanisms of spinal cord astrocyte biology in health and disease.

4.2. Human iPSC-Derived Ventral Spinal Cord-like Astrocytes Provide an Improved Experimental System for Lower Motor Neuron Disease Research

A number of a priori requirements need to be fulfilled by human iPSC-derived astrocytes before they can be deemed suitable for the study of astrocyte involvement in lower motor neuron degeneration in ALS, as well as other lower motor neuron diseases. At a minimum, these cells must exhibit molecular hallmarks of ventral brainstem/spinal cord astrocytes, because the latter are the specific astrocyte subtypes that functionally interact with lower motor neurons. As already addressed, the human iPSC-derived VS astrocyte preparations described in this study fulfill this requirement.

Lower motor neuron disease-relevant astrocyte preparations should also display defined biological properties in order to qualify as an informative experimental system to investigate astrocyte-associated mechanisms of ALS pathophysiology. As a start, they should facilitate the investigation of genes for which an altered expression has been associated with ALS phenotypes. For instance, the expression of two channels found on astrocytic endfeet, the inward rectifier-type potassium channel family member, KCNJ10, and the water channel, AQP4, is affected in opposite ways in animal ALS models, where KCNJ10 levels are decreased whereas AQP4 levels are increased [55,56,74–76]. Consistently, KCNJ10 is downregulated in astrocytes derived from ALS patients with mutations in the *SOD1* gene [48]. The abnormal expression of AQP4 has been associated with altered blood–brain barrier integrity in ALS patients, as well as impaired potassium homeostasis and glutamate dysregulation [76,77]. Based on these observations, we examined the expression of both *KCNJ10* and *AQP4* in human iPSC-derived VS astrocytes. We observed that these preparations express low levels of *AQP4*, suggesting that they should be suited to investigate the functional impact of *AQP4* up-regulation, a situation that might be expected in astrocytes generated from iPSCs derived from ALS patients. Conversely, human iPSC-derived VS astrocytes express detectable levels of *KCNJ10*, implying that they might provide an informative experimental system to investigate the functional consequence of *KCNJ10* down-regulation, which was observed in astrocytes from ALS patients. Both of these lines of studies would be challenging if astrocytes expressing high levels of *AQP4* or low levels of *KCNJ10*, respectively, were used. Although these are only two examples, they provide grounds for the discussion of broader properties expected of astrocyte preparations with potential to offer disease-relevant experimental models.

Another trait that would be expected a priori for disease-relevant iPSC-derived astrocytes is the lack of intrinsic activation in the absence of internal or external insults. This feature would facilitate the investigation of abnormal astrogliosis mechanisms, such as those associated with ALS [25–27]. The present work has suggested that human iPSC-derived VS astrocytes do not exhibit obvious signs of activation, as implied by the low or undetectable expression of a number of previously described astrogliosis markers, such as *SRGN*, *IL1B*, *TNFA*, *CCL2*, and *CXCL10*, as well as low levels of *AQP4*, as already described. The presence of well-organized F-actin stress fibers is also consistent with a non-reactive phenotype.

In summary, the present findings provide evidence that human iPSC-derived VS astrocytes have a mature phenotype characterized by the expression of genes typical of differentiated ventral spinal cord astrocytes, and display both spontaneous and induced Ca^{2+} signaling, without exhibiting obvious signs of activation. The availability of a protocol enabling relatively rapid generation from human iPSCs of astrocytes with properties resembling those of astrocytes in the ventral spinal cord will begin to address the challenges brought about by the demonstrated functional heterogeneity of astrocytes in the brain and spinal cord [4,6,8], the selected contributions of different types of astrocytes to neuronal degeneration in ALS and other neurodegenerative disease [78–80], and the need

for fast and robust derivation strategies yielding disease-relevant preparations of specific astrocyte subtypes.

Supplementary Materials: The following are available online at https://www.mdpi.com/article/10.3390/cells11030399/s1, Video S1: Spontaneous calcium waves; Video S2: ATP-induced calcium waves.

Author Contributions: V.S. performed all microscopy experiments, data analysis, and figure preparation. V.S. and L.G. performed qPCR experiments. M.C., G.H. and A.K.F.F. induced iPSCs into neural progenitor cells. V.S. performed astrocyte differentiation and maturation. S.S., T.M.D., V.S. and G.R. conceived the overall study plan. S.S. and T.M.D. supervised the study. S.S. and V.S. wrote the manuscript. All authors have read and agreed to the published version of the manuscript.

Funding: S.S. and G.R. were supported by funding from ALS Canada/Brain Canada Hudson Translational Team Grant. T.M.D. received funding to support this project through the Canada First Research Excellence Fund, awarded through the Healthy Brains, Healthy Lives initiative at McGill University and the CQDM FACs program. Additional funding was provided by the Canadian Institutes for Health Research and Fonds de la recherche en Sante-Quebec under the frame of E-Rare-3, the ERA-Net for Research on Rare Diseases (SS).

Institutional Review Board Statement: This study was conducted in accordance with the Declaration of Helsinki, and the use of human iPSCs in this research was approved by the McGill University Health Centre Research Ethics Board (DURCAN_IPSC/2019-5374).

Informed Consent Statement: Informed consent was obtained from all subjects involved in the study.

Data Availability Statement: Not applicable.

Acknowledgments: We thank Louise Thiry, Nisha Pulimood, Yeman Tang, Rita Lo, Gilles Maussion, and Valerio Piscopo for discussions, advice and assistance.

Conflicts of Interest: The authors declare no competing interests.

References

1. Wahis, J.; Hennes, M.; Arckens, L.; Holt, M.G. Star power: The emerging role of astrocytes as neuronal partners during cortical plasticity. *Curr. Opin. Neurobiol.* **2021**, *67*, 174–182. [CrossRef] [PubMed]
2. Tan, C.X.; Burrus Lane, C.J.; Eroglu, C. Role of astrocytes in synapse formation and maturation. *Curr. Top. Dev. Biol.* **2021**, *142*, 371–407. [PubMed]
3. Han, R.T.; Kim, R.D.; Molofsky, A.V.; Liddelow, S.A. Astrocyte-immune cell interactions in physiology and pathology. *Immunity* **2021**, *54*, 211–224. [CrossRef] [PubMed]
4. Bayraktar, O.A.; Fuentealba, L.C.; Alvarez-Buylla, A.; Rowitch, D.H. Astrocyte Development and Heterogeneity. *Cold Spring Harb. Perspect. Biol.* **2014**, *7*, a020362. [CrossRef]
5. Tabata, H. Diverse subtypes of astrocytes and their development during corticogenesis. *Front. Neurosci.* **2015**, *9*, 114. [CrossRef]
6. Khakh, B.S.; Deneen, B. The Emerging Nature of Astrocyte Diversity. *Annu. Rev. Neurosci.* **2019**, *42*, 187–207. [CrossRef]
7. De Majo, M.; Koontz, M.; Rowitch, D.; Ullian, E.M. An update on human astrocytes and their role in development and disease. *Glia* **2020**, *68*, 685–704. [CrossRef]
8. Zhang, Y.; Barres, B.A. Astrocyte heterogeneity: An underappreciated topic in neurobiology. *Curr. Opin. Neurobiol.* **2010**, *20*, 588–594. [CrossRef]
9. Oberheim, N.A.; Goldman, S.A.; Nedergaard, M. Heterogeneity of astrocytic form and function. *Methods Mol. Biol.* **2012**, *814*, 23–45.
10. Lundgaard, I.; Osório, M.J.; Kress, B.T.; Sanggaard, S.; Nedergaard, M. White matter astrocytes in health and disease. *Neuroscience* **2014**, *276*, 161–173. [CrossRef]
11. Yoon, H.; Walters, G.; Paulsen, A.R.; Scarisbrick, I.A. Astrocyte heterogeneity across the brain and spinal cord occurs developmentally, in adulthood and in response to demyelination. *PLoS ONE* **2017**, *12*, e0180697. [CrossRef] [PubMed]
12. Jurga, A.M.; Paleczna, M.; Kadluczka, J.; Kuter, K.Z. Beyond the GFAP-Astrocyte Protein Markers in the Brain. *Biomolecules* **2021**, *11*, 1361. [CrossRef] [PubMed]
13. Krencik, R.; Zhang, S.C. Directed differentiation of functional astroglial subtypes from human pluripotent stem cells. *Nat. Protoc.* **2011**, *6*, 1710–1717. [CrossRef] [PubMed]
14. Emdad, L.; D'Souza, S.L.; Kothari, H.P.; Qadeer, Z.A.; Germano, I.M. Efficient differentiation of human embryonic and induced pluripotent stem cells into functional astrocytes. *Stem Cells Dev.* **2012**, *21*, 404–410. [CrossRef]
15. Shaltouki, A.; Peng, J.; Liu, Q.; Rao, M.S.; Zeng, X. Efficient generation of astrocytes from human pluripotent stem cells in defined conditions. *Stem Cells* **2013**, *31*, 941–952. [CrossRef]

16. Paşca, A.M.; Sloan, S.A.; Clarke, L.E.; Tian, Y.; Makinson, C.D.; Huber, N.; Kim, C.H.; Park, J.Y.; O'Rourke, N.A.; Nguyen, K.D.; et al. Functional cortical neurons and astrocytes from human pluripotent stem cells in 3D culture. *Nat. Methods* **2015**, *12*, 671–678. [CrossRef]
17. Tcw, J.; Wang, M.; Pimenova, A.A.; Bowles, K.R.; Hartley, B.J.; Lacin, E.; Machlovi, S.I.; Abdelaal, R.; Karch, C.M.; Phatnani, H.; et al. An Efficient Platform for Astrocyte Differentiation from Human Induced Pluripotent Stem Cells. *Stem Cell Rep.* **2017**, *9*, 600–614. [CrossRef]
18. Cook, C.; Petrucelli, L. Genetic Convergence Brings Clarity to the Enigmatic Red Line in ALS. *Neuron* **2019**, *101*, 1057–1069. [CrossRef]
19. Mejzini, R.; Flynn, L.L.; Pitout, I.L.; Fletcher, S.; Wilton, S.D.; Akkari, P.A. ALS Genetics, Mechanisms, and Therapeutics: Where Are We Now? *Front Neurosci.* **2019**, *13*, 1310. [CrossRef]
20. Kim, G.; Gautier, O.; Tassoni-Tsuchida, E.; Ma, X.R.; Gitler, A.D. ALS Genetics: Gains, Losses, and Implications for Future Therapies. *Neuron* **2020**, *108*, 822–842. [CrossRef]
21. McAlary, L.; Chew, Y.L.; Lum, J.S.; Geraghty, N.J.; Yerbury, J.J.; Cashman, N.R. Amyotrophic Lateral Sclerosis: Proteins, Proteostasis, Prions, and Promises. *Front Cell. Neurosci.* **2020**, *14*, 581907. [CrossRef] [PubMed]
22. Serio, A.; Patani, R. Concise Review: The Cellular Conspiracy of Amyotrophic Lateral Sclerosis. *Stem Cells* **2018**, *36*, 293–303. [CrossRef] [PubMed]
23. Izrael, M.; Slutsky, S.G.; Revel, M. Rising Stars: Astrocytes as a Therapeutic Target for ALS Disease. *Front. Neurosci.* **2020**, *14*, 824. [CrossRef] [PubMed]
24. Vahsen, B.F.; Gray, E.; Thompson, A.G.; Ansorge, O.; Anthony, D.C.; Cowley, S.A.; Talbot, K.; Turner, M.R. Non-neuronal cells in amyotrophic lateral sclerosis–From pathogenesis to biomarkers. *Nat. Rev. Neurol.* **2021**, *17*, 333–348. [CrossRef]
25. Van Damme, P.; Bogaert, E.; Dewil, M.; Hersmus, N.; Kiraly, D.; Scheveneels, W.; Bockx, I.; Braeken, D.; Verpoorten, N.; Verhoeven, K.; et al. Astrocytes regulate GluR2 expression in motor neurons and their vulnerability to excitotoxicity. *Proc. Natl. Acad. Sci. USA* **2007**, *104*, 14825–14830. [CrossRef]
26. Tripathi, P.; Rodriguez-Muela, N.; Klim, J.R.; de Boer, A.S.; Agrawal, S.; Sandoe, J.; Lopes, C.S.; Ogliari, K.S.; Williams, L.A.; Shear, M.; et al. Reactive Astrocytes Promote ALS-like Degeneration and Intracellular Protein Aggregation in Human Motor Neurons by Disrupting Autophagy through TGF-β1. *Stem Cell Rep.* **2017**, *9*, 667–680. [CrossRef]
27. Varcianna, A.; Myszczynska, M.A.; Castelli, L.M.; O'Neill, B.; Kim, Y.; Talbot, J.; Nyberg, S.; Nyamali, I.; Heath, P.R.; Stopford, M.J.; et al. Micro-RNAs secreted through astrocyte-derived extracellular vesicles cause neuronal network degeneration in C9orf72 ALS. *EBioMedicine* **2019**, *40*, 626–635. [CrossRef]
28. Grad, L.I.; Rouleau, G.A.; Ravits, J.; Cashman, N.R. Clinical Spectrum of Amyotrophic Lateral Sclerosis (ALS). *Cold Spring Harb. Perspect. Med.* **2017**, *7*, a024117. [CrossRef] [PubMed]
29. Nijssen, J.; Comley, L.H.; Hedlund, E. Motor neuron vulnerability and resistance in amyotrophic lateral sclerosis. *Acta Neuropathol.* **2017**, *133*, 863–885. [CrossRef]
30. Ragagnin, A.M.G.; Shadfar, S.; Vidal, M.; Jamali, M.S.; Atkin, J.D. Motor Neuron Susceptibility in ALS/FTD. *Front Neurosci.* **2019**, *13*, 532. [CrossRef]
31. Stifani, S. Taking Cellular Heterogeneity into Consideration when Modeling Astrocyte Involvement in Amyotrophic Lateral Sclerosis Using Human Induced Pluripotent Stem Cells. *Front. Cell. Neurosci.* **2021**, *15*, 707861. [CrossRef] [PubMed]
32. Chen, C.X.; Abdian, N.; Maussion, G.; Thomas, R.A.; Demirova, I.; Cai, E.; Tabatabaei, M.; Beitel, L.K.; Karamchandani, J.; Fon, E.A.; et al. A Multistep Workflow to Evaluate Newly Generated iPSCs and Their Ability to Generate Different Cell Types. *Methods Protoc.* **2021**, *4*, 50. [CrossRef] [PubMed]
33. Du, Z.W.; Chen, H.; Liu, H.; Lu, J.; Qian, K.; Huang, C.L.; Zhong, X.; Fan, F.; Zhang, S.C. Generation and expansion of highly pure motor neuron progenitors from human pluripotent stem cells. *Nat. Commun.* **2015**, *6*, 6626. [CrossRef] [PubMed]
34. Thiry, L.; Hamel, R.; Pluchino, S.; Durcan, T.; Stifani, S. Characterization of Human iPSC-derived Spinal Motor Neurons by Single-cell RNA Sequencing. *Neuroscience* **2020**, *450*, 57–70. [CrossRef]
35. Methot, L.; Soubannier, V.; Hermann, R.; Campos, E.; Li, S.; Stifani, S. Nuclear factor-kappaB regulates multiple steps of gliogenesis in the developing murine cerebral cortex. *Glia* **2018**, *66*, 2659–2672. [CrossRef]
36. Soubannier, V.; Maussion, G.; Chaineau, M.; Sigutova, V.; Rouleau, G.; Durcan, T.M.; Stifani, S. Characterization of human iPSC-derived astrocytes with potential for disease modeling and drug discovery. *Neurosci Lett.* **2020**, *731*, 135028. [CrossRef]
37. Schmittgen, T.D.; Livak, K.J. Analyzing real-time PCR data by the comparative C(T) method. *Nat Protoc.* **2008**, *3*, 1101–1108. [CrossRef]
38. Moein, M.; Grzyb, K.; Martins, T.G.; Komoto, S.; Peri, F.; Crawford, A.D.; D'Herouel, A.F.; Skupin, A. CaSiAn: A Calcium Signaling Analyzer tool. *Bioinformatics* **2018**, *34*, 3052–3054. [CrossRef]
39. Krumlauf, R. Hox genes, clusters and collinearity. *Int. J. Dev. Biol.* **2018**, *62*, 659–663. [CrossRef]
40. Pearson, J.C.; Lemons, D.; McGinnis, W. Modulating Hox gene functions during animal body patterning. *Nat. Rev. Genet.* **2005**, *6*, 893–904. [CrossRef]
41. Bradley, R.A.; Shireman, J.; McFalls, C.; Choi, J.; Canfield, S.G.; Dong, Y.; Liu, K.; Lisota, B.; Jones, J.R.; Petersen, A.; et al. Regionally specified human pluripotent stem cell-derived astrocytes exhibit different molecular signatures and functional properties. *Development* **2019**, *146*, dev170910. [CrossRef] [PubMed]

42. Hou, P.S.; hAilín, D.Ó.; Vogel, T.; Hanashima, C. Transcription and Beyond: Delineating FOXG1 Function in Cortical Development and Disorders. *Front. Cell. Neurosci.* **2020**, *14*, 35. [CrossRef] [PubMed]
43. Sagner, A.; Briscoe, J. Establishing neuronal diversity in the spinal cord: A time and a place. *Development* **2019**, *146*, dev182154. [CrossRef] [PubMed]
44. Leung, B.; Shimeld, S.M. Evolution of vertebrate spinal cord patterning. *Dev. Dyn.* **2019**, *248*, 1028–1043. [CrossRef]
45. Wichterle, H.; Lieberam, I.; Porter, J.A.; Jessell, T.M. Directed differentiation of embryonic stem cells into motor neurons. *Cell* **2002**, *110*, 385–397. [CrossRef]
46. Hochstim, C.; Deneen, B.; Lukaszewicz, A.; Zhou, Q.; Anderson, D.J. Identification of positionally distinct astrocyte subtypes whose identities are specified by a homeodomain code. *Cell* **2008**, *133*, 510–522. [CrossRef]
47. Olsen, M.L.; Campbell, S.L.; Sontheimer, H. Differential distribution of Kir4.1 in spinal cord astrocytes suggests regional differences in K+ homeostasis. *J. Neurophysiol.* **2007**, *98*, 786–793. [CrossRef]
48. Kelley, K.W.; Ben Haim, L.; Schirmer, L.; Tyzack, G.E.; Tolman, M.; Miller, J.G.; Tsai, H.H.; Chang, S.M.; Molofsky, A.V.; Yang, Y.; et al. Kir4.1-Dependent Astrocyte-Fast Motor Neuron Interactions Are Required for Peak Strength. *Neuron* **2018**, *98*, 306–319.e7. [CrossRef]
49. Pivonkova, H.; Benesova, J.; Butenko, O.; Chvatal, A.; Anderova, M. Impact of global cerebral ischemia on K+ channel expression and membrane properties of glial cells in the rat hippocampus. *Neurochem. Int.* **2010**, *57*, 783–794. [CrossRef]
50. Olsen, M.L.; Campbell, S.C.; McFerrin, M.B.; Floyd, C.L.; Sontheimer, H. Spinal cord injury causes a wide-spread, persistent loss of Kir4.1 and glutamate transporter 1: Benefit of 17 beta-oestradiol treatment. *Brain* **2010**, *133 Pt 4*, 1013–1025. [CrossRef]
51. Leo, M.; Schmitt, L.I.; Steffen, R.; Kutritz, A.; Kleinschnitz, C.; Hagenacker, T. Modulation of Glutamate Transporter EAAT1 and Inward-Rectifier Potassium Channel Kir4.1 Expression in Cultured Spinal Cord Astrocytes by Platinum-Based Chemotherapeutics. *Int. J. Mol. Sci.* **2021**, *22*, 6300. [CrossRef] [PubMed]
52. Nagelhus, E.A.; Mathiisen, T.M.; Ottersen, O.P. Aquaporin-4 in the central nervous system: Cellular and subcellular distribution and coexpression with KIR4.1. *Neuroscience* **2004**, *129*, 905–913. [CrossRef] [PubMed]
53. Strohschein, S.; Hüttmann, K.; Gabriel, S.; Binder, D.K.; Heinemann, U.; Steinhäuser, C. Impact of aquaporin-4 channels on K+ buffering and gap junction coupling in the hippocampus. *Glia* **2011**, *59*, 973–980. [CrossRef]
54. Ikeshima-Kataoka, H. Neuroimmunological Implications of AQP4 in Astrocytes. *Int. J. Mol. Sci.* **2016**, *17*, 1306. [CrossRef] [PubMed]
55. Bataveljić, D.; Nikolić, L.; Milosević, M.; Todorović, N.; Andjus, P.R. Changes in the astrocytic aquaporin-4 and inwardly rectifying potassium channel expression in the brain of the amyotrophic lateral sclerosis SOD1(G93A) rat model. *Glia* **2012**, *60*, 1991–2003. [CrossRef] [PubMed]
56. Kaiser, M.; Maletzki, I.; Hülsmann, S.; Holtmann, B.; Schulz-Schaeffer, W.; Kirchhoff, F.; Bähr, M.; Neusch, C. Progressive loss of a glial potassium channel (KCNJ10) in the spinal cord of the SOD1 (G93A) transgenic mouse model of amyotrophic lateral sclerosis. *J. Neurochem.* **2006**, *99*, 900–912. [CrossRef] [PubMed]
57. Liddelow, S.A.; Barres, B.A. Reactive Astrocytes: Production, Function, and Therapeutic Potential. *Immunity* **2017**, *46*, 957–967. [CrossRef]
58. Clarke, L.E.; Liddelow, S.A.; Chakraborty, C.; Munch, A.E.; Heiman, M.; Barres, B.A. Normal aging induces A1-like astrocyte reactivity. *Proc. Natl. Acad. Sci. USA* **2018**, *115*, E1896–E1905. [CrossRef]
59. Liddelow, S.A.; Guttenplan, K.A.; Clarke, L.E.; Bennett, F.C.; Bohlen, C.J.; Schirmer, L.; Bennett, M.L.; Münch, A.E.; Chung, W.S.; Peterson, T.C.; et al. Neurotoxic reactive astrocytes are induced by activated microglia. *Nature* **2017**, *541*, 481–487. [CrossRef]
60. Zamanian, J.L.; Xu, L.; Foo, L.C.; Nouri, N.; Zhou, L.; Giffard, R.G.; Barres, B.A. Genomic analysis of reactive astrogliosis. *J. Neurosci.* **2012**, *32*, 6391–6410. [CrossRef]
61. John, G.R.; Chen, L.; Rivieccio, M.A.; Melendez-Vasquez, C.V.; Hartley, A.; Brosnan, C.F. Interleukin-1beta induces a reactive astroglial phenotype via deactivation of the Rho GTPase-Rock axis. *J. Neurosci.* **2004**, *24*, 2837–2845. [CrossRef] [PubMed]
62. Hillen, A.E.J.; Burbach, J.P.H.; Hol, E.M. Cell adhesion and matricellular support by astrocytes of the tripartite synapse. *Prog. Neurobiol.* **2018**, *165*, 66–86. [CrossRef] [PubMed]
63. Hansson, E. Actin filament reorganization in astrocyte networks is a key functional step in neuroinflammation resulting in persistent pain: Novel findings on network restoration. *Neurochem. Res.* **2015**, *40*, 372–379. [CrossRef] [PubMed]
64. Tyzack, G.E.; Hall, C.E.; Sibley, C.R.; Cymes, T.; Forostyak, S.; Carlino, G.; Meyer, I.F.; Schiavo, G.; Zhang, S.-C.; Gibbons, G.M.; et al. A neuroprotective astrocyte state is induced by neuronal signal EphB1 but fails in ALS models. *Nat. Commun.* **2017**, *8*, 1164. [CrossRef]
65. Shigetomi, E.; Patel, S.; Khakh, B.S. Probing the Complexities of Astrocyte Calcium Signaling. *Trends Cell. Biol.* **2016**, *26*, 300–312. [CrossRef]
66. Bazargani, N.; Attwell, D. Astrocyte calcium signaling: The third wave. *Nat. Neurosci.* **2016**, *19*, 182–189. [CrossRef]
67. Adami, R.; Bottai, D. Spinal Muscular Atrophy Modeling and Treatment Advances by Induced Pluripotent Stem Cells Studies. *Stem Cell Rev. Rep.* **2019**, *15*, 795–813. [CrossRef]
68. Halpern, M.; Brennand, K.J.; Gregory, J. Examining the relationship between astrocyte dysfunction and neurodegeneration in ALS using hiPSCs. *Neurobiol. Dis.* **2019**, *132*, 104562. [CrossRef]
69. Slanzi, A.; Iannoto, G.; Rossi, B.; Zenaro, E.; Constantin, G. In vitro Models of Neurodegenerative Diseases. *Front. Cell Dev. Biol.* **2020**, *8*, 328. [CrossRef]

70. Hawrot, J.; Imhof, S.; Wainger, B.J. Modeling cell-autonomous motor neuron phenotypes in ALS using iPSCs. *Neurobiol. Dis.* **2020**, *134*, 104680. [CrossRef]
71. Hall, C.E.; Yao, Z.; Choi, M.; Tyzack, G.E.; Serio, A.; Luisier, R.; Harley, J.; Preza, E.; Arber, C.; Crisp, S.J.; et al. Progressive Motor Neuron Pathology and the Role of Astrocytes in a Human Stem Cell Model of VCP-Related ALS. *Cell Rep.* **2017**, *19*, 1739–1749. [CrossRef] [PubMed]
72. Roybon, L.; Lamas, N.J.; Garcia, A.D.; Yang, E.J.; Sattler, R.; Lewis, V.J.; Kim, Y.A.; Kachel, C.A.; Rothstein, J.D.; Przedborski, S.; et al. Human stem cell-derived spinal cord astrocytes with defined mature or reactive phenotypes. *Cell Rep.* **2013**, *4*, 1035–1048. [CrossRef] [PubMed]
73. Zhao, C.; Devlin, A.C.; Chouhan, A.K.; Selvaraj, B.T.; Stavrou, M.; Burr, K.; Brivio, V.; He, X.; Mehta, A.R.; Story, D.; et al. Mutant C9orf72 human iPSC-derived astrocytes cause non-cell autonomous motor neuron pathophysiology. *Glia* **2020**, *68*, 1046–1064. [CrossRef] [PubMed]
74. Nicaise, C.; Soyfoo, M.S.; Authelet, M.; De Decker, R.; Bataveljic, D.; Delporte, C.; Pochet, R. Aquaporin-4 overexpression in rat ALS model. *Anat. Rec.* **2009**, *292*, 207–213. [CrossRef]
75. Cui, Y.; Masaki, K.; Yamasaki, R.; Imamura, S.; Suzuki, S.O.; Hayashi, S.; Sato, S.; Nagara, Y.; Kawamura, M.F.; Kira, J. Extensive dysregulations of oligodendrocytic and astrocytic connexins are associated with disease progression in an amyotrophic lateral sclerosis mouse model. *J. Neuroinflamm.* **2014**, *11*, 42. [CrossRef]
76. Zou, S.; Lan, Y.L.; Wang, H.; Zhang, B.; Sun, Y.G. The potential roles of aquaporin 4 in amyotrophic lateral sclerosis. *Neurol. Sci.* **2019**, *40*, 1541–1549. [CrossRef]
77. Ng Kee Kwong, K.C.; Mehta, A.R.; Nedergaard, M.; Chandran, S. Defining novel functions for cerebrospinal fluid in ALS pathophysiology. *Acta Neuropathol. Commun.* **2020**, *8*, 140. [CrossRef]
78. Gomes, C.; Sequeira, C.; Barbosa, M.; Cunha, C.; Vaz, A.R.; Brites, D. Astrocyte regional diversity in ALS includes distinct aberrant phenotypes with common and causal pathological processes. *Exp. Cell Res.* **2020**, *395*, 112209. [CrossRef]
79. Mishra, V.; Re, D.B.; Le Verche, V.; Alvarez, M.J.; Vasciaveo, A.; Jacquier, A.; Doulias, P.T.; Greco, T.M.; Nizzardo, M.; Papadimitriou, D.; et al. Systematic elucidation of neuron-astrocyte interaction in models of amyotrophic lateral sclerosis using multi-modal integrated bioinformatics workflow. *Nat. Commun.* **2020**, *11*, 5579. [CrossRef]
80. Song, Y.J.; Halliday, G.M.; Holton, J.L.; Lashley, T.; O'Sullivan, S.S.; McCann, H.; Lees, A.J.; Ozawa, T.; Williams, D.R.; Lockhart, P.J.; et al. Degeneration in different parkinsonian syndromes relates to astrocyte type and astrocyte protein expression. *J. Neuropathol. Exp. Neurol.* **2009**, *68*, 1073–1083. [CrossRef]